Numerical Modeling of Space Plasma Flows: ASTRONUM-2012
ASP Conference Series, Vol. 474
N. V. Pogorelov, E. Audit, and G. P. Zank, eds.

Modeling Source Surface Plasma and Magnetic Field Based on Expansion Factor f_S and Angular Distance θ_b Between the Foot Points

Fang Shen[1,2], Xueshang Feng[1], Changqing Xiang[1] and S. T. Wu[2]

[1]*SIGMA Weather Group, State Key Laboratory of Space Weather, Center for Space Science and Applied Research, Chinese Academy of Sciences, Beijing 100190, China*

[2]*Center for Space Plasma and Aeronomic Research, The University of Alabama in Huntsville, Huntsville, AL 35899 USA*

Abstract. The purpose of this paper is to model the distribution of plasma and magnetic field on the source surface of 2.5 R_S covering four different phases of solar activity. We use the expansion factor f_S and the angular distance θ_b in specifying the solar wind speed on the source surface, which can separate the open field region and the close field region effectively. We select 136 Carrington Rotations (CRs) covering four different phases of solar activity, and use an empirical model of the magnetic field topology by Wilcox Solar Observatory (WSO) and an empirically derived global coronal density distribution by MKIII in High Altitude Observatory (HAO) as input. The solar wind speed at 1AU derived from the new distribution on the source surface works much better than one derived from the previous method (Shen et al. 2010), as compared with observational data.

1. Introduction

Recently, the global distribution for the corona plasma and magnetic field near 2.5 R_S was studied numerically in our previous paper (Shen et al. 2010), in which the solar wind speed at 1 AU deduced from the speed on the source surface of 2.5 R_S existed much discrepancy compared with the observation. Here, much improvement is made to remedy the discrepancy. The expansion factor f_S and the angular distance θ_b are introduced to empirically specify the open field region and the close field region by considering the magnetic field topology effects (Feng et al. 2010, 2011).

The expansion factor f_S (Wang et al. 1990) has the form of $f_S = (R_S/r)^2(B_{R_S}/B_r)^2$, where R_S and r are the solar radius and the distance from the solar center; and B_{R_S} and B_r are magnetic field strength at the solar surface (1 R_S) and at r. The angular distance θ_b denotes the minimum angular separation (at the photosphere) between an open field foot point and its nearest coronal hole boundary, which could be calculated from the magnetic field distribution and tracking the magnetic field lines from solar surface to source surface. We can use it to distinguish the high-speed solar winds from the low-speed solar wind (high-speed stream originating from the center of an open field region has large θ_b and low-speed stream from the hole boundary has a small θ_b).

In the present paper, we use the expansion factor f_S and the angular distance θ_b in specifying the solar wind speed on the source surface to separate the open field region and the close field region effectively. We also derived the solar wind speed at 1AU from the new distribution on the source surface, which works much better than the one derived from the previous method (Shen et al. 2010).

2. Statistical and Numerical Study

Here, we select 136 CRs (CRs 1811 to 1946) which spans the middle latter portion of solar cycle 22 (January, 1989 - April, 1995) and the former portion of solar cycle 23 (May, 1995 - March, 1999). The selected CRs can be broadly grouped into four categories according to the solar activities (Shen et al. 2010): the solar maximum (CRs 1811 - 1825), the descending phase (CRs 1826 - 1904), the solar minimum (CRs 1905 - 1925) and the ascending phase (CRs 1926 - 1946). We determine the distributions of the radial magnetic field B_r at 2.5 R_S for every CR by using the line-of-sight (los) photospheric field (B_{los}) measurements, which was made at Wilcox Solar Observatory (WSO), and the potential field source surface (PFSS) model (Zhao et al. 2006; Hu et al. 2008). We adopt the global density distribution at 2.5 R_S from the observational data of K coronal polarized brightness (pB) by MKIII in High Altitude Observatory (HAO). Following the solar wind density model constructed by Guhathakurta et al. (1996), we can give the coronal density from 1 R_S to 5.5 R_S roughly (Shen et al. 2010). The magnetic structure and the density distribution on the source surface of 2.5 R_S evolve during the four phases of the solar cycle were illustrated in the Figure 2 by Shen et al. (2010).

Then, we can achieve the solar wind speed at 2.5 R_S by considering the magnetic field expansion factor f_S and the angular distance θ_b. The PFSS model (Zhao et al. 2006; Hu et al. 2008) was used to determine f_S and θ_b at 2.5 R_S. And beyond 2.5 R_S, f_S and θ_b take their distributions on the source surface (Feng et al. 2010, 2011). The following empirical relationship ((Owens et al. 2005); also used by Feng et al. (2010)) is used to assign solar wind speed at a radius of 5 R_S in this study: $V(f_S, \theta_b) = 265 + \frac{1.5}{1+f_S^{2/7}}(5.8 - 1.6e^{[1-(\theta_b/7.5)^3]})^{3.5}$ km/s with the help the expansion factor f_S and the angular distance θ_b (with the unit of degree). Fig. 1 displays the distribution of the number density, the magnetic field, the expansion factor f_S and the angular distance θ_b at 2.5 R_S, during CR 1823 (at the solar maximum, (a)), CR 1874 (at the descending phase, (b)), CR 1910 (at the solar minimum, (c)) and CR 1932 (at the ascending phase, (d)), respectively.

The solar wind speed at 2.5 R_S can be derived from the physical conditions at 5 R_S by using the mass conservation relation. Fig. 2 gives the average radial solar wind speed distribution on the source surface over the four phases of solar activity. Then, the average solar plasma mass flux can be obtained by,

$$F_{m_i}(2.5\mathrm{Rs}, \theta, \varphi) = [n(2.5\mathrm{Rs}, \theta, \varphi)v(2.5\mathrm{Rs}, \theta, \varphi)]_i (i = 1, 2, 3, 4),$$

on the source surface over the four phases, according to the observations of the K coronal brightness and the solar plasma speed, where $(n(2.5\mathrm{Rs}, \theta, \varphi)v(2.5\mathrm{Rs}, \theta, \varphi))_i$ denote the average solar plasma mass flux at 2.5 R_S over the maximum ($i = 1$), the descending phase ($i = 2$), the minimum ($i = 3$) and the ascending phase ($i = 4$), separately.

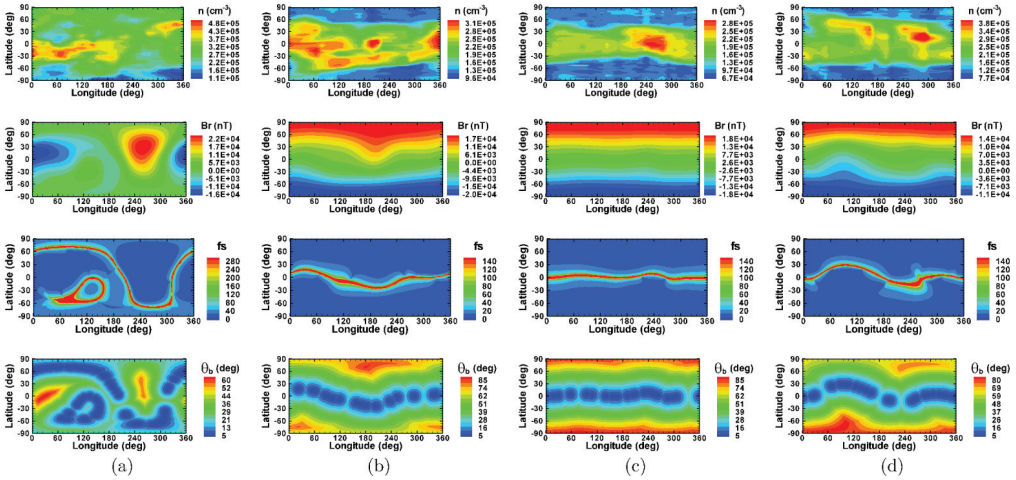

Figure 1. Distribution of the number density n, the magnetic field B_r, the expansion factor f_S and the angular distance θ_b at 2.5 R_S during (a) CR 1823 (maximum), (b) CR 1874 (descending phase), (c) CR 1910 (minimum) and (d) CR 1932 (ascending phase), respectively.

Based on the statistical average results of the magnetic field, the density and the coronal mass outputs flux pattern at 2.5 R_S for the four different phases of solar activities, we can write the self-consistent model for coronal physical parameters on the source surface in 1D ideal MHD equations (Wei et al. 2003; Shen et al. 2010):

$$v\frac{\partial v}{\partial r} + n\frac{\partial v}{\partial r} + 2nv/r = 0, \tag{1}$$

$$nv\frac{\partial v}{\partial r} + \frac{\partial P}{\partial r} + ng = 0, \tag{2}$$

$$n\frac{\partial p}{\partial r} - \gamma p\frac{\partial n}{\partial r} = 0 \tag{3}$$

$$r\frac{\partial B}{\partial r} + 2B = 0 \tag{4}$$

$$p = 2\Re' nT \tag{5}$$

$$\frac{\partial p}{\partial r} = 2\Re' T\frac{\partial n}{\partial r} + 2\Re' n\frac{\partial T}{\partial r} \tag{6}$$

$$\beta(B) = 8\pi p/B^2 \tag{7}$$

$$nv = F_{m_c}(F_{m_i}, f_s, \theta_b) \tag{8}$$

here equations (1)-(7) were used in Shen et al. (2010), in which equation (7) was the statistical results for the plasma beta β and γ=1.4. From the previous studies by Arge et al. (2003) and Owens et al. (2005), there exist the inverse correlation between the expansion factor f_S and speed, and positive correlation between the angular distance θ_b and speed. In this paper, in order to deduce the speed at 2.5 R_S, we chose the following

function: $F_{m_c}(F_{m_i}, f_s, \theta_b) = F_{m_i} \frac{\theta_b^{0.2}}{(1+f_s)^{1/3}}$; $v_r\,|_{r=2.5Rs} = F_{m_c}/n$. This correction to the solar plasma mass flux will make the correspondence between the coronal current sheet and the small velocity region; and between the polar coronal hole and the large velocity region, more obviously during all the solar cycle. In this function, i = 1, 2, 3 and 4 denote the average solar plasma mass flux over the maximum, the descending phase, the minimum and the ascending phase of solar activity, separately. It is a function of three coronal parameters, the average coronal mass outputs flux (F_{m_i}), the expansion factor (f_S) and the angular distance (θ_b, measured in degrees). This relationship quite differs from that in our previous work (Shen et al. 2010).

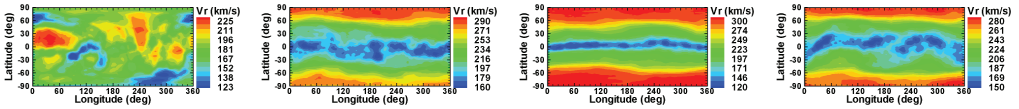

Figure 2. Average distributions of the radial solar speed at 2.5 R_S over the four different phases: (a) maximum, (b) descending phase, (c) minimum and (d) ascending phase of solar activities.

The other 10 unknown parameters, B, $\partial B/\partial r$, v, $\partial v/\partial r$, T, $\partial T/\partial r$, n, $\partial n/\partial r$, p and $\partial p/\partial r$, can be found if any two of them are known by solving governing equations (1)-(8). In the case investigated, the magnetic field B and density n are two known inputs on the source surface at 2.5 R_S, which are calculated in the previous section. In the following computation, the source surface is divided into 182×92 cells with each being $2^\circ \times 2^\circ$.

3. Results

The numerical results of the solar wind parameters, such as the temperature and the radial velocity on the source surface can be deduced during every CR at the solar maximum, the descending phase, the solar minimum, and the ascending phase, based on the statistical average distributions of B_r, n, and the coronal mass flux F_{m_c} on the source surface at 2.5 R_S, and the self-consistent MHD equations mentioned above.

From top to bottom, Fig. 3 gives the numerical results of global distribution for the temperature T, the radial velocity v_r and the value F_{m_i}/n on the source surface of 2.5 R_S during CR 1823 (i = 1, (a)), CR 1874 (i = 2, (b)), CR 1910 (i = 3, (c)) and CR 1932 (i = 4, (d)), respectively. For comparison, the coronal current sheets in the panels are shown with the white lines. From the top two rows in Fig. 3, we find the minimum temperature and velocity region are related to the coronal current sheet region at the solar minimum, the descending phase, the ascending phase and the solar maximum. The high temperature and velocity regions, with most of the low density regions, are basically located at the polar coronal hole regions, the temperature and radial speed shown in the top two rows of Fig. 2 together with the location of the coronal current sheets. In addition, we can observe that where the solar activity level increases, the high speed stream area reduces while the high density area changes reversely. From comparing the middle and the bottom rows of Fig. 2, there exist obvious differences between F_{m_i}/n (speed without correction) and v_r. With correction to the average coronal mass outputs

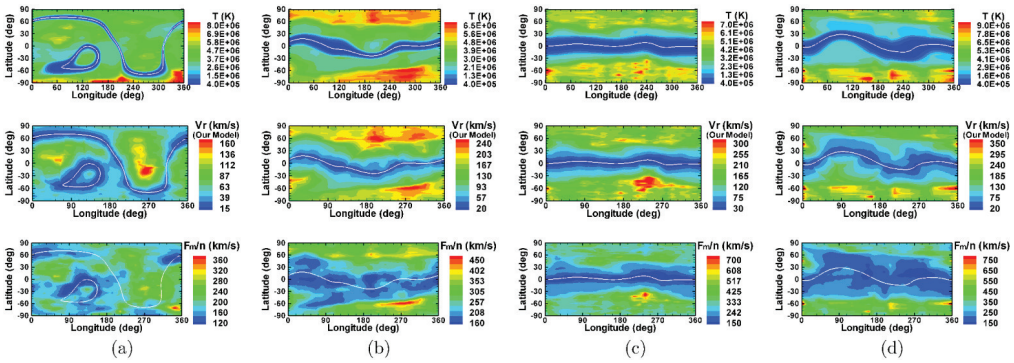

Figure 3. Distribution of the temperature, the radial velocity v_r, and the value F_{m_i}/n on source surface of 2.5 R_S from numerical simulation at (a) CR 1823 in 1989 (maximum); (b) CR 1874 in 1993 (descending phase); (c) CR 1910 in 1996 (minimum); and (d) CR 1932 in 1998 (ascending phase). The white lines in each panel denote the coronal current sheets.

flux F_{m_i}, the velocity can show the obvious correspondence between the coronal current sheet and the small velocity region; and between the polar coronal hole and the large velocity region, during all the solar cycle. We can find that the lower-speed region (corresponding to coronal current sheet region) in the bottom panels are quite thinner than that in the middle panels.

Then, we obtain the solar wind speed at 1 AU by mapping the speed on the source surface of 2.5 R_S to that at the earth orbit through a linear relation:$v(1AU) = c_1 \times v(2.5Rs) + 255$, where (1) $c_1 = 3.15$ at the solar maximum; (2) $c_1 = 4.65$ at the descending and ascending phases; and (3) $c_1 = 9.15$ at the solar minimum. The coefficient c_1 is estimated by means of the radial speed relation of the solar wind (Withbroe et al. 1988). We were also interested in comparing our improved numerical speed at 1 AU with observational data, WSA model and that in our previous model (Shen et al. 2010). Fig. 4 compares the solar wind speed at 1 AU observed by IMP 8 (1989) and WIND (1995, 1997 and 1998) (red) with solar wind speed predictions from the present model (black), the previous model (blue) and using the WSA velocity relationship (Arge et al. 2003) (green), $V(f_S, \theta_b) = 265 + \frac{25}{f_S^{2/7}}(5.0 - 1.1e^{[1-(\theta_b/4)^2]})^2$ km/s, Here, both f_S and θ_b are calculated based on the WSO data, which were analyzed in detail in Part 2. Solar wind speed predictions obtained by the improved numerical model show better agreement with observations and the WSA model than those obtained in our previous model (see Fig. 4). The improved model provides a clear improvement over the previous model in all solar phases, including the solar maximum (a), the descending phase (b), the solar minimum (c) and the ascending phase (d).

Most of the highest observed solar wind speeds are due to the passage of Interplanetary Coronal Mass Ejections (ICMEs) excluded from improved numerical model. Despite the presence of ICMEs, the black curves can reproduce many of the recurring high speed streams. In this context, the self-consistent, global distributions on the source surface of 2.5 R_S during all the phases of solar cycle could be used for understanding the change of the interplanetary condition.

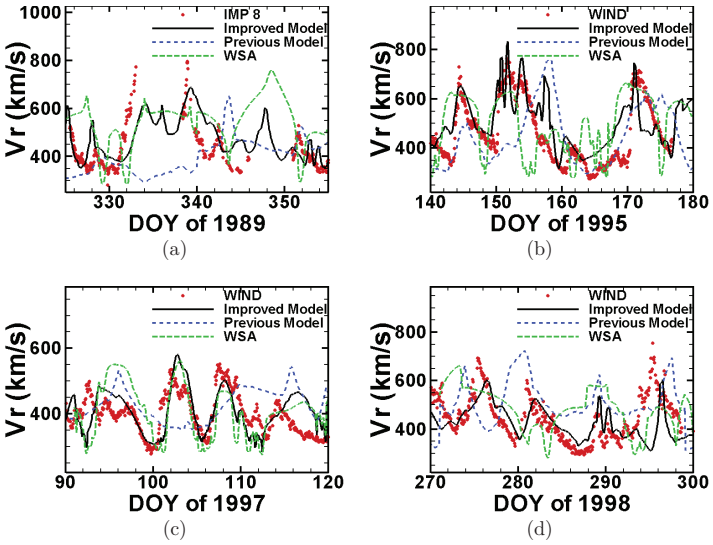

Figure 4. Comparison of solar wind speed predictions from our present model (black lines) and our previous model (blue dashed lines), the observational speed (red dots) and the simulated speed by WSA model (green long-dashed lines) at 1 AU during four time intervals: (a) DOY 325 - 355 of 1989; (b) DOY 140 - 180 of 1995; (c) DOY 90 - 120 of 1997; and (d) DOY 270 - 300 of 1998.

4. Summary

In this study, we have modeled the distribution of plasma and magnetic field on the source surface of 2.5 R_S covering four different phases of solar activity by involving the topological effect of f_S and θ_b. We analyze the coronal mass outputs and numerically study the self-consistent global distribution on the source surface for 136 CRs covering four different phases of solar activity. Finally, we also estimate the solar wind speed at 1 AU as a simple function of the speed on the source surface. By comparing the results from this model with observational data, we find that the solar wind speed deduced from this improved model works much better than the previous model. The magnetic field expansion factor f_S and the angular distance θ_b can be used to separate the open - close field area on the source surface more effectively. Further we will use this improved self-consistent source surface model during all phases of solar cycle as an inner-boundary condition for 3D MHD simulation, and use it to improve the capability of 3D MHD model for predicting the interplanetary condition.

Acknowledgments. It should be acknowledged that the contours of K corona white light brightness at 1.36 R_S are obtained from the Mauna Loa Solar Observatory, solar photospheric magnetic field data are from WSO, and solar wind speeds at 1 AU are taken from the observation data of Wind spacecraft and IMP 8 satellite. The work performed by F. Shen, X. Feng and C. Xiang is jointly supported by the National Basic Research Program (973 program) under grant 2012CB825601, the Knowledge Innovation Program of the Chinese Academy of Sciences (KZZD-EW-01-4), the National Natural Science Foundation of China (41074121, 41174150 and 41031066), the Specialized Research Fund for State Key Laboratories and the Public science and technol-

ogy research funds projects of ocean (201005017). S. T. Wu and F. Shen are supported by NSF (AGS 1153323) and NASA EPSCOR (NNX09AP74A).

References

Arge, C. N., D. Odstrcil, V. J. Pizzo& L. R. Mayer 2003 Solar Wind Ten, AIP Conference Proceedings, 679, 190
Feng, X., L. P. Yang, C. Q. Xiang et al. 2010 Astrophys. J., 723, 300
Feng, X., Zhang, S., Xiang, C., Yang, L., Jiang, C.& Wu, S. T., 2011 Astrophys. J., 734, 50
Guhathakurta, M., Holzer, T. E.& MacQueen, R. M. 1996 Astrophys. J., 459, 817
Hu, Y., Feng, X., Wu, S. T.& Song, W. 2008 J. Geophys. Res., 113, A03106
Owens, M. J., Arge, C. N., Spence, H. E.& Pembroke, A., 2005 J. Geophys. Res., 110, A12105
Shen, F., Feng, X., Xiang, C.& Song, W. B. 2010 Journal of Atmospheric and Solar-Terrestrial Physics, 72(13), 1008
Wang, Y. M.& Sheeley Jr., N.R. 1990 Astrophys. J., 355, 726
Wei, F. S., X. S. Feng, H. C. Cai & Q. J. Zhou 2003 J. Geophys. Res., 108(A6), 1238
Withbroe, G. L. 1988 Astrophys. J., 325, 442
Zhao, X. P., Hoeksema, J. T., Liu, Y.& Scherrer, P. H. 2006 J. Geophys. Res., 111, A10108